

Broadband computation of the scattering coefficients of infinite arbitrary cylindersCédric Blanchard,^{1,2,*} Brahim Guizal,¹ and Didier Felbacq¹¹*Laboratoire Charles Coulomb, University of Montpellier 2, 34071 Montpellier, France*²*Department of Applied Physics, University of Granada, 18071 Granada, Spain*

(Received 25 February 2012; published 26 July 2012)

We employ a time-domain method to compute the near field on a contour enclosing infinitely long cylinders of arbitrary cross section and constitution. We therefore recover the cylindrical Hankel coefficients of the expansion of the field outside the circumscribed circle of the structure. The recovered coefficients enable the wideband analysis of complex systems, e.g., the determination of the radar cross section becomes straightforward. The prescription for constructing such a numerical tool is provided in great detail. The method is validated by computing the scattering coefficients for a homogeneous circular cylinder illuminated by a plane wave, a problem for which an analytical solution exists. Finally, some radiation properties of an optical antenna are examined by employing the proposed technique.

DOI: [10.1103/PhysRevE.86.016711](https://doi.org/10.1103/PhysRevE.86.016711)

PACS number(s): 02.70.–c

I. INTRODUCTION

The study of electromagnetic (EM) wave interaction with particles is enjoying an increasing level of popularity. Scientists from a wide variety of disciplines—including atmospheric physics, electrical engineering, nanotechnology, etc.—are faced with problems involving light scattering. The scattering problem of a plane wave falling upon a homogeneous circular cylinder at perpendicular incidence was first solved by Lord Rayleigh in 1881 [1]. The problem has therefore been thoroughly explored, and the solutions for more complicated configurations—viz., oblique incidence, elliptical cylinders, concentric cylinders—were consecutively given. The scattered cylindrical waves are usually expressed by infinite series that involve Bessel functions. Each term of the expansion is weighted by a scattering coefficient that contains the information about the amplitude and phase of the corresponding partial wave. The series converge slowly when the radius of the object is appreciable compared to the wavelength. Techniques such as the Watson transformation (see [2], p. 784) enable the solution to be converted into rapidly convergent series.

Deviating from the above-mentioned ideal configurations considerably complicates the derivation of the general solution. For aggregates of cylinders, the scattered field for an individual object is an incoming wave from the other clusters' perspective, resulting in a challenging problem. The analytical solution for the scattering of two infinitely long, parallel cylinders of different radii and materials at oblique incidence has been given in [3], while a theory of scattering by a finite number of cylinders of arbitrary cross section is presented in [4]. The complete general solution for aggregates of spheres has been derived by Xu [5], who obtained the expansion coefficients for all the particles through the resolution of a large number of linear equations by an asymptotic iteration method. The use of computational resources is unavoidable in the last two references; hence the corresponding techniques can be considered as semianalytical.

Light diffraction by arbitrary-shaped and/or inhomogeneous objects becomes insurmountable to work out by an analytical treatment. As a result, numerical methods must be

employed. The counterpart is that the spatial discretization makes the knowledge of the EM field sparse while, most importantly, the size of the computational domain cannot be extended at will. The former issue can be overcome by using interpolation techniques from the values at the neighboring grid points (a simple Lagrangian interpolation is often sufficient). The latter can constitute a significant problem given that it prevents the determination of the EM field far away from the scatterer.

In this paper we use the Transmission Line Modeling (TLM) time-domain method [6–8] to compute the near field scattered by an arbitrary finite aggregate of cylinders (not necessarily circular). Then we recover the scattering coefficients by integration along a circular contour that encloses the scatterers. With these coefficients it is in particular possible to calculate the diffracted field everywhere outside the computational domain. Note that we are dealing with concepts that differ from the so-called near-to-far-field transformation [9,10], for the distance from the scatterers to the point of observation is not considered as infinite. The proposed method is rather similar to that used in [11] (but in this reference, the Bessel functions are actually replaced by their large-argument asymptotic expansions) and [12], in which the scattering coefficients of an antenna are determined from measurements, made with a probe, of the near fields on a cylinder containing the antenna. In contrast to our method, these two works were, however, of experimental nature while the source was restricted to emit cylindrical waves.

The extension of our method to three-dimensional structures is conceptually identical to the developments reported in this paper, albeit much more computationally demanding. The results and prescriptions presented here are useful given that cylindrical particles are not uncommon in nature, while applications based on arrays of micro- or nanorods are diverse. In addition, it should be noted that many problems involving cylindrical structures can be treated adequately within the framework of infinite cylinder theory [13].

II. SCATTERING COEFFICIENTS OF THE EXPANSION

We shall suppose an infinite cylinder of radius R_{cyl} to be embedded in an infinite and homogeneous medium. The

*cedric@ugr.es

propagation constants in these media are denoted k and k_1 , respectively. The cylinder axis is taken to coincide with the z axis. The object is illuminated by a linearly polarized wave with its electric vector parallel to the z axis, i.e., the polarization is transverse magnetic. The cross section of the cylinder is arbitrary, while there is no restriction on the constitutive parameters (permittivity ϵ , permeability μ , and conductivity σ). The expansion of the complex spatial form of the scattered field, which propagates in the outward direction, can be represented by cylindrical wave functions:

$$\vec{E}^s = \hat{z} \sum_{n=-\infty}^{\infty} a_n H_n^{(2)}(k_1 r) \exp(in\phi), \quad (1)$$

where $H_n^{(2)}$ are the Hankel functions of the second kind, while r and ϕ are the radial and angular cylindrical coordinates, respectively. The choice of $e^{i\omega t}$ as the time convention to denote the time-harmonic dependence is made, which leads to the use of Hankel functions of the second kind. The determination of the expansion coefficients a_n is the key to the problem as they ensure the knowledge of the scattered EM field. This turns out to be a trivial task if the cross section is circular and the cylinder homogeneous. However, if these conditions are no longer realized, the a_n may be tough to derive.

We propose to numerically calculate the a_n and then, by using Eq. (1), to obtain \vec{E}^s as a continuous function of r and ϕ . Multiplying Eq. (1) by $e^{-ip\phi}$, integrating over a closed circular contour \mathcal{C} of radius $R > R_{\text{cyl}}$, and with the help of orthogonality relations, we readily obtain

$$a_n = \frac{\frac{1}{2\pi} \int_0^{2\pi} E_z^s(R, \phi) \exp(-in\phi) d\phi}{H_n^{(2)}(k_1 R)}. \quad (2)$$

It is plain from Eq. (2) that knowledge of E_z^s over \mathcal{C} allows the calculation of the expansion coefficients. The problem is therefore reduced to the determination of $E_z^s(R, \phi)$ which can be calculated by numerical simulation. At first examination, Eq. (2) seems to suggest that the a_n coefficients depend on R . Nevertheless, this is certainly not the case because in the rigorous derivation of Eq. (2) one should be able to use any circumference to perform the integration and then obtain the a_n coefficients. A way to figure this out is to notice that the R dependence is in both the numerator (through the scattered field on the contour) and the denominator (through the Hankel functions). This overall makes the coefficients independent of R . On the other hand, the integral in Eq. (2) will be obtained numerically over the perimeter of the circle of radius R , i.e., the sample points $E_z^s(R, \phi(i))$ will be taken over a contour whose length is $2\pi R$. Therefore, it is obvious that the smaller R is, the closer the samples are to each other, i.e., the better the estimation of the integral. To summarize, although the a_n do not depend on R , it is better to choose the latter as small as possible. Note also that choosing R to be small goes together with a minimal TLM computational window.

To give more generality to our approach, it is judicious to chose a time-domain technique to perform the calculation. A time-domain method directly calculates the impulse response of an EM system; as a result a single simulation provides broadband temporal wave forms. In our problem, this means

we have access to the a_n in terms of the frequency in a single simulation. We have chosen to carry out this calculation with TLM, which is recognized as a powerful method for scattering problems in the realm of EM [14] as well as acoustics [15]. The very versatile TLM Symmetrical Condensed Node is employed so that the polarization of the incident wave can be changed to transverse electric with almost no impact on the numerical implementation [7].

III. NUMERICAL IMPLEMENTATION

The numerical calculation of the integral of Eq. (2) is of no difficulty. However, it must be ensured that the number of samples that describes \mathcal{C} is large enough to reach a reasonable precision. By using interpolation, as will be explained in the next paragraph, we can evaluate the integrand at as many points as desired. In our calculation, the field is calculated at every 0.1° of \mathcal{C} , that is $E_z^s(R, \phi)$ is calculated at 3600 different locations. In contrast, we have verified that scanning \mathcal{C} with a 1° step may not be enough, depending on the frequency under consideration.

The spatial discretization usually involves Cartesian elementary cells, called nodes in the TLM jargon. Even though lattices made up of Cartesian nodes have proven to be flexible and robust, certain bodies are more accurately modeled by means of other coordinate systems. A cylinder with circular cross section would be judiciously simulated by employing a cylindrical grid for which the elementary cells are cylinders whose cross sections are plane figures bounded by two radii and the arcs of two concentric circles. Cylindrical grids prevent the undesirable staircase approximations in the modeling of a curved object, improving the numerical simulation of certain devices [16], but are unadapted to the modeling of other configurations such as aggregates of scatterers. That is the reason why this work has been performed with Cartesian nodes; there is however a counterpoint: the use of interpolation is unavoidable. This statement arises from the fact that the EM field is computed at the centers of the Cartesian nodes while the path of \mathcal{C} does not necessarily coincide with those particular locations. In the following, we will use a simple Lagrangian interpolation of order 3—i.e., the nine closest nodes (three along the x direction and three along the y direction) are involved.

The incident electric field is modeled by the Gaussian time function source

$$f(t) = e^{-G^2(t-t_0)^2}, \quad (3)$$

where G allows control of the width of the pulse in the time domain. The time wave form of the pulse is centered at time t_0 . This common low-pass source condition radiates a numerical signal that is then altered, in the mesh, by the presence of any modification of the specified EM parameters in the grid. A Fourier analysis of the complete time histories of this radiation, obtained in a single run, provides the field over a wide frequency band that spreads out from direct current regime to an arbitrary high-frequency regime. Note, however, that the latter is restricted by the specifications of the TLM grid, e.g., the size of the nodes and the value of the refractive index of the simulated medium, as well as the value of G . What is more, using Eq. (3) as source directly provides the

magnitude and phase of the field, which is interesting given that Eq. (2) requires $E_z^s(R, \phi)$ to be expressed in its complex form. There is a remaining question: assuming such a low-pass source, what is the relation between the numerical values that are obtained at all points of the grid and the physical electric field? We suppose that the pulse of Eq. (3) is generated at the origin and propagates along the x direction in free space, i.e., with velocity c_0 . Furthermore, we assume the source to generate a plane wave form. If we define the Fourier transform as $\frac{1}{\sqrt{\pi}} \int_{-\infty}^{+\infty} f(t) \exp(-i\omega t)$ (note the minus sign in the argument of the exponential to conform to the $e^{i\omega t}$ time convention), we readily obtain $\mathcal{F}[f(t)] = \frac{e^{-i\omega t_0 - \frac{\omega^2}{4G^2}}}{G}$. At coordinate x , the pulse should be of the form $e^{-G^2(t-t_0-t_{\text{ret}})^2}$, where $t_{\text{ret}} = x/c_0 = k_0 x/\omega$. It is obvious that the Fourier transform of this new function differs from $\mathcal{F}[f(t)]$ by a slight modification in the exponential's argument: t_0 must be substituted by $(t_0 + t_{\text{ret}})$. The ratio of the new Fourier transform to $\mathcal{F}[f(t)]$ yields the expression $e^{-i\omega t_{\text{ret}}} = e^{-ik_0 x}$, which precisely corresponds to the spatial part of an individual harmonic component of an electric field that propagates along the x direction. In conclusion, each harmonic of the computed signal must be divided by the corresponding harmonic of the incident signal to recover the complex scattered field. Note that it is important to take into account the eventual phase shift that results from the spatial distance between the location of the source and the origin (in the literature, the analytical derivations of the diffraction of a plane wave by a circular infinite cylinder usually assume that the center of the cross section is located at the origin).

IV. VALIDATION OF THE METHOD

In order to validate the proposed technique, we first consider that the scattering cylinder is homogeneous and has a circular cross section. For the sake of simplicity, we suppose that the relative permittivity of the cylinder, of radius $R_{\text{cyl}} = 20$ nm, is constant in the whole operating frequency range (a dispersive case will be examined in the next section) and amounts to $\epsilon = 4$. Concerning the numerical specifications, the dimensions of the TLM nodes are $\Delta l = \Delta x = \Delta y = 1$ nm, while $G = 10^{15} \text{ s}^{-1}$ and $t_0 = 3.6/G$ s. The cylinder is located at the center of the computational grid, which is a square whose sides are 200 nm long. A uniform plane wave, whose electric field is linearly polarized along the z direction, is normally incident upon the cylinder. The plane wave source is realized by employing the total-field-scattered-field technique (also referred to as the Huygens' technique): the lattice is divided into an outer and an inner region in which only the scattered and total field, respectively, are computed (see [9], p. 186). By locating \mathcal{C} in the scattered-fields region, the scattered field is directly obtained.

The prescriptions of Sec. III allow the computation of the expansion coefficients a_n for each sampled frequency. By using Eq. (1), the scattered field—as a continuous function of r and ϕ , and for the number of frequencies that depend on the length of the temporal source signal—can thus be determined. In Fig. 1, the real and imaginary parts of the scattered electric field (blue and red circles, respectively) for $r = 200$ nm and $\phi = 0$

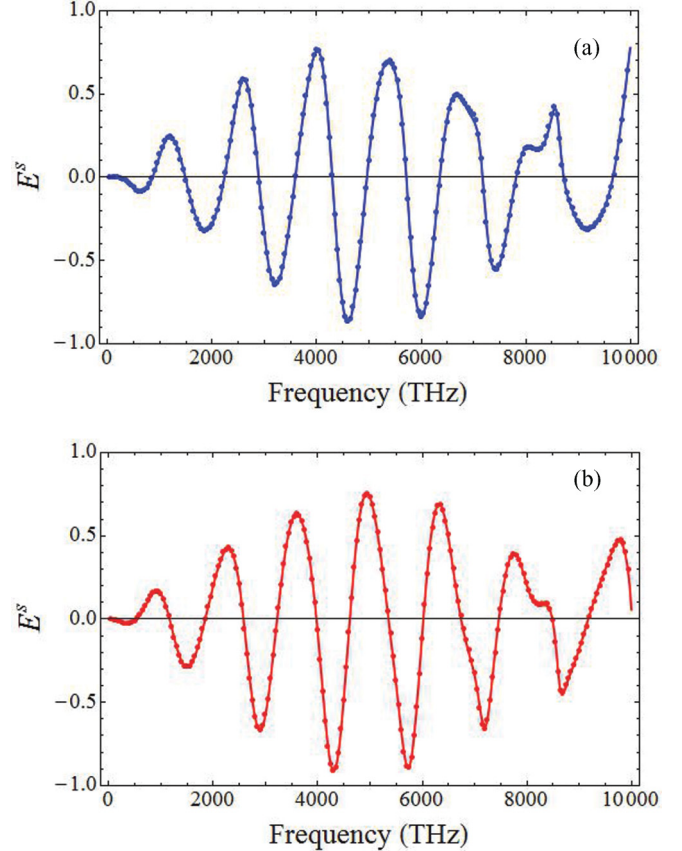


FIG. 1. (Color online) (a) Real part and (b) imaginary part of the scattered electric field in terms of frequency by a homogeneous circular cylinder at the point of observation $r = 200$ nm and $\phi = 0$. The continuous lines represent the analytical result while the markers represent the numerical calculation.

(note that this point is outside the mesh) are plotted in terms of frequency. It is worth stressing that the series of Eq. (1) is infinite; the truncation must be treated with care if we want the field to converge. The numerical calculation can be compared with the well-known analytical solution [17], which has been plotted in the same figures (continuous lines). The agreement is good irrespective of the frequency, which validates the present approach. The highest frequency, 10^4 THz, corresponds to the wavelength $\lambda = 30$ nm in vacuum, which is of the order of magnitude of R_{cyl} and much larger than Δl . Hence, we can make the assumption that such a wavelength is not small enough to reveal the actual staircase shape of the simulated object far away from it. However, this result may no longer be true in the near-field region.

V. OPTICAL ANTENNA ILLUMINATED BY CYLINDRICAL RADIATION

The proposed technique is especially useful if the analytical calculation is complex to derive or even unavailable. In the present section, we focus on a complex structure that can serve as an optical antenna. The device is depicted in the inset of Fig. 2; it consists of two silver nanocylinders (of radius $R_{\text{Ag}} = 30$ nm, gray color) and a dielectric nanocylinder (of radius $R_{\text{diel}} = 250$ nm, blue color). The distance between the centers

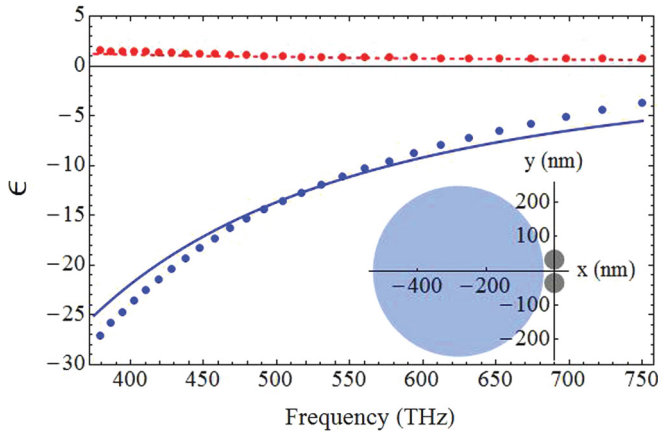


FIG. 2. (Color online) Complex permittivity of silver in terms of frequency. Blue solid line, real part; red dashed line, imaginary part. The continuous lines represent the values that have been employed in our simulation while the points are values taken from Palik [18]. Inset: scheme of the simulated structure; the line source is equidistantly located between the two silver cylinders (gray color).

of the two metallic structures is 68 nm, while $x_{\text{diel}} = -280$ nm. A similar system, involving spherical particles, was investigated in depth by Devilez and colleagues in [19], where it was shown that such an optical antenna exhibits high directionality in the optical spectrum. Regarding potential experimental realization of this hybrid antenna, it is worth noting that the main difficulty would lie in the short distance, 8 nm, between the two metallic particles. However, techniques allowing gaps of less than 5 nm have already been proposed. Let us mention, for instance, the assembly of noble-metal nanoparticles on DNA scaffolds [20] or gold nanoparticle dimer resonators coated with active antibodies [21].

In our simulation, we suppose that $\epsilon_{\text{diel}} = 2$ in the whole optical spectrum ranging from 400 to 800 THz. Concerning the metallic particles, the permittivity is set to the negative value -11.32 at 545.455 THz, in agreement with Palik [18]. For the other frequencies the permittivity is governed by the inherent dispersion that occurs in the TLM nodes for the modeling of negative refractive index materials. It was established in [22] that such permittivity is of the form $\epsilon(\omega) = 1 - \omega_p^2/\omega^2$, where ω_p represents the plasma angular frequency, which can be determined by knowledge of a particular point of the curve $\epsilon(\omega)$. We shall suppose the conductivity of the silver cylinders to be constant; its value is set to $\sigma = 25\,329$ S/m. In Fig. 2 the resulting silver complex permittivity is plotted and compared to the values provided by Palik; it appears that the silver cylinder is correctly modeled in the optical spectrum in spite of these approximations.

The incoming wave was thus far a plane wave. Interaction between fields radiated by other sources, such as a simple line source or a Gaussian or Bessel [23] beam, and any kind of structures can also be investigated by means of our approach. In this section the optical antenna is illuminated by a line source generating waves radiating in the outward direction. The source is equidistantly located between the two silver cylinders, at the origin. Furthermore, the computational impressed electric field has the temporal form given by Eq. (3). If there is no scatterer the propagating EM field should be isotropic:

we first positively verify that, in that case, all the coefficients of the expansion but the zero-order one amount to zero.

The natural application of the proposed method is the retrieval of fields far away from the excited object by means of the computation of the scattering coefficients. However, the knowledge of the a_n is beneficial in various other aspects such as the specification of the system in terms of a multipole expansion, for each of the terms in the scattered-field expansion in Eq. (1) can be viewed as the partial component of an oscillatory multipole [24]. It is of interest to characterize them in order, for instance, to detect the dominant partial modes of the radiation or the resonant frequencies. In Fig. 3(a) the amplitude of the a_n (normalized to the corresponding maximum value) at 100 THz is represented;

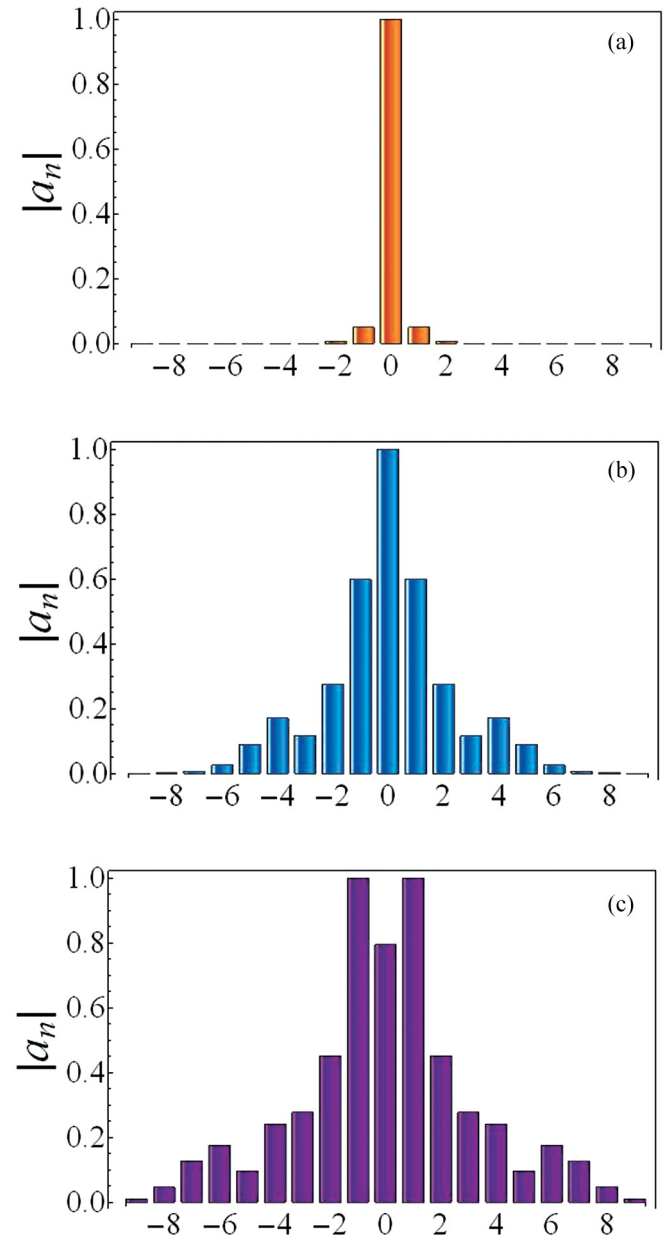


FIG. 3. (Color online) Normalized amplitude of the scattering coefficients for the individual partial modes at (a) 100, (b) 500, and (c) 700 THz.

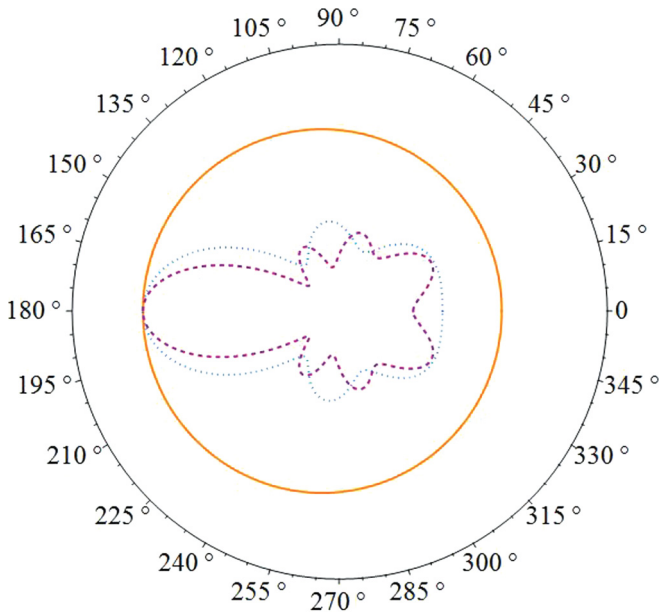


FIG. 4. (Color online) Radiation diagram at $r = 8000$ nm. Orange solid line, 100 THz; blue dotted line, 500 THz; purple dashed line, 700 THz.

the first mode turns out to be highly dominant. The radiation is therefore isotropic around this low frequency. When the frequency increases other modes are excited. This is evinced in Figs. 3(b) and 3(c) which represent the relative amplitudes of the a_n at 500 and 700 THz, respectively. Accordingly, the radiation is expected to become anisotropic. The radiation diagram in Fig. 4 confirms that the radiation is isotropic at 100 THz, while a fairly high directionality around 180° is observed at 500 and 700 THz. This directionality stresses

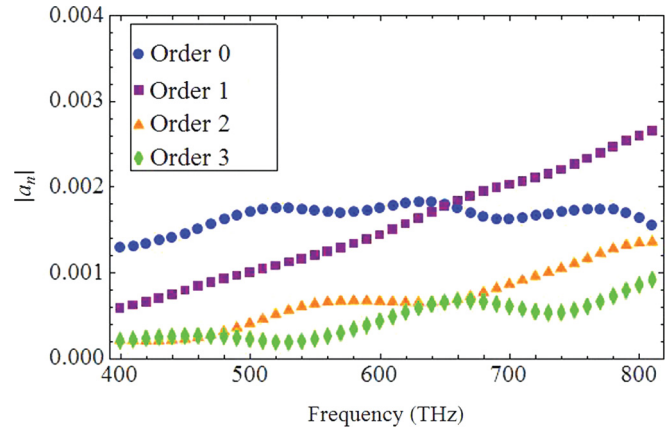


FIG. 5. (Color online) First four orders of the a_n .

the function of the near-field lens of the dielectric particle. In Fig. 5, the antenna scattering coefficients are plotted in terms of frequency for the first four orders. It permits one to get a clear picture of the elementary cylindrical modes that are involved in the scattering process. For example one can identify the frequency bands where the zero order—which leads to isotropic radiation—is dominant.

VI. CONCLUSION

We have proposed a detailed prescription for the computation of the scattering coefficients of any two-dimensional system. We have shown that using a time-domain method, such as the TLM, has the virtue of directly revealing the broadband response of the diffraction phenomenon. The approach allows the calculation of the field everywhere in space but is also useful to characterize the system through the individual behavior of the partial oscillations.

- [1] Lord Rayleigh, *Philos. Mag.* **12** (1881).
- [2] J. A. Kong, *Electromagnetic Wave Theory*, 3rd ed. (EMW Publishing, Cambridge, MA, 2008).
- [3] H. A. Yousif and S. Köhler, *J. Opt. Soc. Am. A* **5**, 1085 (1988).
- [4] D. Felbacq, G. Tayeb, and D. Maystre, *J. Opt. Soc. Am. A* **11**, 2526 (1994).
- [5] Y. L. Xu, *Appl. Opt.* **34**, 4573 (1995).
- [6] P. B. Johns and R. L. Beurle, *Proc. Inst. Electr. Eng.* **118**, 1203 (1971).
- [7] P. B. Johns, *IEEE Trans. Microwave Theory Tech.* **35**, 370 (1987).
- [8] C. Christopoulos, *The Transmission-Line Modeling Method: TLM* (Oxford University Press, Oxford, 1995).
- [9] A. Taflov and S. C. Hagness, *Computational Electrodynamics: The Finite-Difference Time-Domain Method*, 3rd ed. (Artech House, Norwood MA, 2005).
- [10] R. Luebbers, D. Ryan, and J. Beggs, *IEEE Trans. Antennas Propag.* **40**, 848 (1992).
- [11] W. M. Leach and D. T. Paris, *IEEE Trans. Antennas Propag.* **21**, 435 (1973).
- [12] R. Rammal, M. Lalande, E. Martinod, N. Feix, M. Jouvét, J. Andrieu, and B. Jecko, *Int. J. Antennas Propag.* **2009**, Article ID 798473 (2009).
- [13] C. F. Bohren and D. R. Huffman, *Absorption and Scattering of Light by Small Particles* (John Wiley & Sons, New York, 1983).
- [14] C. Eswarappa and W. J. R. Hoefler, *IEEE Microwave Guided Wave Lett.* **43**, 4 (1995).
- [15] J. A. Morente and J. A. Portí, *J. Sound Vib.* **241**, 207 (2001).
- [16] C. Blanchard, B.-I. Wu, J. A. Portí, H. Chen, B. Zhang, J. A. Morente, and A. Salinas, *J. Opt. Soc. Am. B* **26**, 2117 (2009).
- [17] C. A. Balanis, *Advanced Engineering Electromagnetics* (John Wiley & Sons, New York, 1989).
- [18] E. D. Palik, *Handbook of Optical Constants of Solids* (Academic Press, New York, 1985).
- [19] A. Devilez, B. Stout, and N. Bonod, *ACS Nano* **6**, 3390 (2010).
- [20] S. Bidault, F. J. García de Abajo, and A. Polman, *J. Am. Chem. Soc.* **130**, 2750 (2008).
- [21] M. Ringler, A. Schwemer, M. Wunderlich, A. Nichtl, K. Kürzinger, T. A. Klar, and J. Feldmann, *Phys. Rev. Lett.* **100**, 203002 (2008).
- [22] C. Blanchard, J. A. Portí, J. A. Morente, and A. Salinas, *Electron. Lett.* **46**, 110 (2010).
- [23] J. Durnin, *J. Opt. Soc. Am. A* **4**, 651 (1987).
- [24] J. A. Stratton, *Electromagnetic Theory*, 1st ed. (McGraw-Hill, New York, 1941).